

# Long-Memory Effects in Linear Response Models of Earth's Temperature and Implications for Future Global Warming

MARTIN RYPDAL AND KRISTOFFER RYPDAL

*Department of Mathematics and Statistics, University of Tromsø, Tromsø, Norway*

(Manuscript received 28 May 2013, in final form 28 March 2014)

## ABSTRACT

A linearized energy-balance model for global temperature is formulated, featuring a scale-invariant long-range memory (LRM) response and stochastic forcing representing the influence on the ocean heat reservoir from atmospheric weather systems. The model is parameterized by an effective response strength, the stochastic forcing strength, and the memory exponent. The instrumental global surface temperature record and the deterministic component of the forcing are used to estimate these parameters by means of the maximum-likelihood method. The residual obtained by subtracting the deterministic solution from the observed record is analyzed as a noise process and shown to be consistent with a long-memory time series model and inconsistent with a short-memory model. By decomposing the forcing record in contributions from solar, volcanic, and anthropogenic activity one can estimate the contribution of each to twentieth-century global warming. The LRM model is applied with a reconstruction of the forcing for the last millennium to predict the large-scale features of Northern Hemisphere temperature reconstructions, and the analysis of the residual also clearly favors the LRM model on millennium time scale. The decomposition of the forcing shows that volcanic aerosols give a considerably greater contribution to the cooling during the Little Ice Age than the reduction in solar irradiance associated with the Maunder Minimum in solar activity. The LRM model implies a transient climate response in agreement with IPCC projections, but the stronger response on longer time scales suggests replacing the notion of equilibrium climate sensitivity by a time scale-dependent sensitivity.

## 1. Introduction

When the climate system is subject to radiative forcing, the planet is brought out of radiative balance and the thermal inertia of the planet makes the surface temperature lag behind the forcing. The time constant  $\tau$ , which is the time for relaxation to a new equilibrium after a sudden change in forcing, has been considered to be an important parameter to determine. The equilibrium climate sensitivity  $S_{\text{eq}}$ , the temperature rise per unit forcing after relaxation is complete, is another. In the industrialized epoch a major source for the present energy imbalance is the steady increase in anthropogenic forcing. If the climate system can be modeled as a hierarchy of interacting subsystems with increasing heat capacities and response times, there will also be a hierarchy of climate

sensitivities. One way of modeling this feature is to replace the standard exponentially decaying impulse-response function  $G(t) \sim e^{-t/\tau}$  with one that is scaling (or scale invariant), that is, decaying like a power law:  $G(t) \sim t^{\beta/2-1}$ . A particular feature of a power law is that it remains a power law with the same exponent under a change of scales. For a climate system that is subject only to random forcing modeled as a white Gaussian noise, the exponential response yields a short-range memory stochastic process. For a scaling response, and if  $0 < \beta < 1$ , the resulting climate variable  $T(t)$  is a long-range memory (LRM) fractional Gaussian noise (fGn) with a power spectral density (PSD) of the form  $\mathcal{P}(f) \sim f^{-\beta}$ . There are several definitions of an LRM process that are mathematically more or less equivalent (Beran 1994; Embrechts and Maejima 2002). For this paper it is natural to define such a process as one resulting from the stochastic integral<sup>1</sup>

 Denotes Open Access content.

*Corresponding author address:* Martin Rypdal, University of Tromsø, N-9037 Tromsø, Norway.  
E-mail: martin.rypdal@uit.no

<sup>1</sup>This stochastic integral is not convergent, and the definition of a continuous-time fGn should therefore only be seen as a formal expression. How to formulate a mathematically well-defined model is discussed in the appendixes.

$$X_{fGn}(t) = \int_{-\infty}^t (t-s)^{\beta/2-1} dB(s). \quad (1)$$

It can be shown that the integrated autocorrelation function (ACF)  $C(\tau)$  for this process is infinite [i.e.,  $\int_0^\infty C(\tau) d\tau = \infty$ ]. This divergence is what defines a long-range memory process. The linear impulse response model is easily Fourier transformed and the modulus of the resulting transfer function is naturally interpreted as a frequency-dependent climate sensitivity  $S(f)$ . In the exponential response model the amplitude response to an oscillation vanishes for high frequencies, but converges to  $S_{eq}$  as  $f \rightarrow 0$ . In the scaling response model  $S(f)$  diverges in the low-frequency limit, indicating high sensitivity of the climate system to low-frequency components of the forcing. We shall demonstrate that long-memory responses can explain important aspects of Northern Hemisphere temperature variability over the last millennium and lead to new predictions of how much more warming there will be “in the pipeline” in any given forcing scenario (Hansen et al. 2005, 2011).

Dozens of papers have been published over the last two decades, demonstrating LRM in temperature records. Many hypothesize that the signal is composed of an LRM noise superposed on a trend driven by external forcing, and hence the methods are designed to eliminate such trends [see a short review and a selection of references in Rypdal et al. (2013)]. The most widely used method is detrended fluctuation analysis (DFA) (Kantelhardt et al. 2001). However, the concept of a slow trend does not always reflect the true nature of deterministic forced variability. Some components of the forcing may be faster than important components of the internal variability, and hence precise separation of internal from forced variability can only be done by using information about the deterministic component of the forcing record. Fortunately, such reconstructions of the forcing records exist and are used as input for historic runs of climate models.

We contend that correct estimation of the LRM properties of the internal climate variability can only be done by analyzing the residual obtained by subtracting the forced deterministic component of the climate signal. We shall show that the climate response function is all we need to predict both the deterministic component of the climate signal and the memory properties of the internal variability.

## 2. Linear response models

Linear response models of Earth’s surface temperature have been considered by several authors [see, e.g., Hansen et al. (2011) and Rypdal (2012)]. The physical backbone is the zero-dimensional, linearized

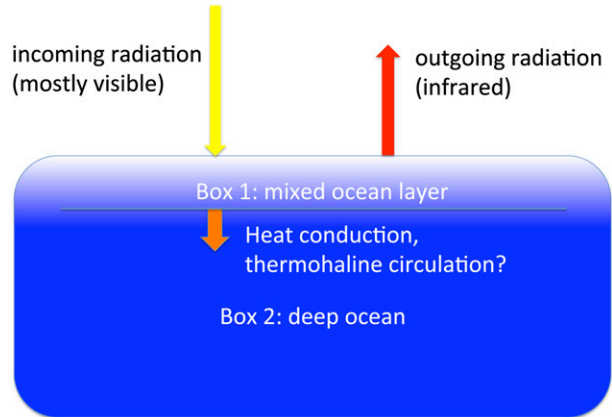


FIG. 1. In a quasi-equilibrium state the surface temperature  $T$  (temperature of mixed layer) can be almost constant while the total influx into the climate system (the deep ocean) is finite. In such a state  $dQ/dt$  in Eq. (1) is nonzero because of an imbalance between the outflux term and influx term on the rhs in this equation.

energy-balance equation derived, for instance, in the appendix of Rypdal (2012). It has the form

$$\frac{dQ}{dt} + \frac{1}{S_{eq}} T = F, \quad (2)$$

where  $Q$  is the total energy content of the climate system;  $F$  and  $T$  are perturbations of radiative influx and surface temperature relative to a reference state in radiative equilibrium, that is, a state where the radiative influx absorbed by the Earth surface balances the infrared radiation emitted to space from the top of the troposphere. It is important to keep in mind that a radiative imbalance can be maintained for a long time with a nearly constant surface temperature if there is a heat transport from the mixed surface layer of the ocean into the slowly warming deep ocean. This situation is illustrated by the cartoon in Fig. 1, where both the atmosphere and the ocean surface layer are close to radiative equilibrium, but the total climate system is not. It can be modeled by a simple and well-known generalization of the one-box energy-balance model to a two-box model:

$$\begin{aligned} C_1 \frac{dT_1}{dt} &= -\frac{1}{S_{eq}} T_1 - \kappa(T_1 - T_2) + F \quad \text{and} \\ C_2 \frac{dT_2}{dt} &= \kappa(T_1 - T_2), \end{aligned} \quad (3)$$

where  $T_1$  could be interpreted as the temperature of the ocean mixed layer,  $T_2$  as the temperature of the deep ocean, and  $C_1$  and  $C_2$  as their respective heat capacities. The parameter  $\kappa$  quantifies the heat transport between the two boxes. For  $C_2 \gg C_1$  the response of  $T_1$  to a unit step in the forcing is

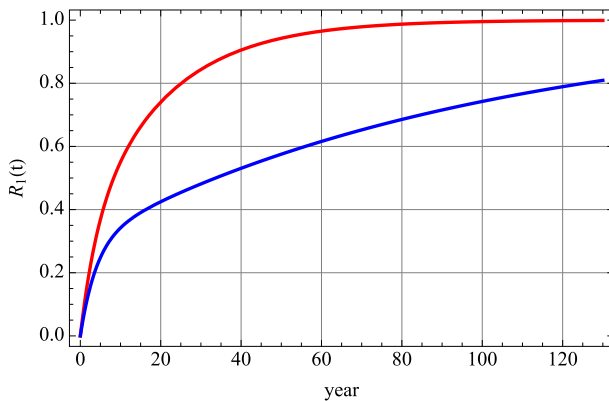


FIG. 2. The red curve is the response function  $R(t)$  for the two-box model with  $\tau_{\text{tr}} = 4$  yr,  $\tau_{\text{eq}} = 20$  yr,  $S_{\text{tr}} = 0.3 \text{ K m}^2 \text{ W}^{-1}$ , and  $S_{\text{eq}} = 1.0 \text{ K m}^2 \text{ W}^{-1}$ . The blue curve for the same parameters but  $\tau_{\text{eq}} = 100$  yr.

$$R(t) \approx S_{\text{tr}}(1 - e^{-t/\tau_{\text{tr}}}) + (S_{\text{eq}} - S_{\text{tr}})(1 - e^{-t/\tau_{\text{eq}}}), \quad (4)$$

where  $S_{\text{tr}}$ ,  $\tau_{\text{tr}}$ , and  $\tau_{\text{eq}}$  are given in terms of the parameters of Eq. (3) (Rypdal 2012). Two examples of this solution are shown in Fig. 2 for different values of the longer time constant. The solution corresponding to a larger separation between the time constants of the mixed layer and the deep ocean could easily be interpreted incorrectly if integrated only up to  $t \sim \tau_{\text{tr}}$ , since the apparent time constant would be  $\tau_{\text{tr}}$  and the sensitivity  $S_{\text{tr}}$ , while the true time constant of the climate system as a whole would be  $\tau_{\text{eq}}$  and the true sensitivity would be  $S_{\text{eq}}$ . This idealized example is of course only an illustration of the principle that slowly responding components of the climate system and slow feedbacks may obscure the notion of equilibrium climate sensitivity. The true equilibrium sensitivity may be much larger than estimated from model runs, and hence future warming following a limited period of persistent forcing may be greater and last longer than predicted from models that do not fully take into account the LRM properties arising from slow responses.

For a given influx the equilibrium outflux is controlled by the Stefan–Boltzmann radiation law and complex feedback processes that determine the equilibrium climate sensitivity  $S_{\text{eq}}$  [see, e.g., Eqs. (A5)–(A7) in Rypdal (2012)]. The true value of  $S_{\text{eq}}$  is subject to considerable controversy because of insufficient knowledge of some of these feedbacks, and because they operate on wildly different time scales (Otto et al. 2013). The estimates of  $S_{\text{eq}}$  are regularly updated in the literature as the global temperature goes through periods of slower or faster warming (Otto et al. 2013; Aldrin et al. 2012). If the climate system responds on a wide range of time scales, the notion of an equilibrium climate sensitivity may be

of little practical interest, since this equilibrium may never be attained in a system that is subject to variability of the forcing. In section 7 we discuss alternatives to this notion.

The exponential response model is obtained from Eq. (2) by introducing an effective heat capacity  $C$  of the climate system such that  $dQ = CdT$ , and introducing the time constant  $\tau = CS_{\text{eq}}$ . Equation (2) then takes the form

$$\mathcal{L}T \equiv C \left( \frac{d}{dt} + \frac{1}{\tau} \right) T = F, \quad (5)$$

where the linear operator  $\mathcal{L}$  has the Green's function

$$G(t) = C^{-1} \exp(-t/\tau), \quad (6)$$

that is, the solution of Eq. (5) is

$$T(t) = \int_{-\infty}^t G(t-s)F(s) ds. \quad (7)$$

In the two-box model  $\mathcal{L}$  is a two-dimensional vector operator acting on the column vector  $(T_1, T_2)^T$ , where the superscript T denotes the transpose, and with a vector Green's function. However, the essential structure of the response function for the surface layer temperature is given by the derivative of Eq. (4):

$$G(t) = \frac{S_{\text{tr}}}{\tau_{\text{tr}}} e^{-t/\tau_{\text{tr}}} + \frac{(S_{\text{eq}} - S_{\text{tr}})}{\tau_{\text{eq}}} e^{-t/\tau_{\text{eq}}}. \quad (8)$$

The simple, linear two-box model contains the essential conceptual elements of our phenomenological response model, since it represents a linear model with more than one relaxation time scale. The state variables are the energy contents of the ocean surface layer and the deep ocean, respectively. The nonlinearities that give rise to the spatiotemporal chaos of the atmosphere and ocean represent unresolved scales that contribute to mean turbulent (anomalous) energy fluxes between the boxes, and to random fluctuations of these fluxes around the mean. The latter represent the stochastic forcing terms. A linear system follows from the ansatz that the mean fluxes are proportional to the temperature difference between the two boxes. The two-box model can trivially be generalized to an  $n$ -box model, whose response function may be designed to mimic a power law up to the slowest relaxation scale. The various boxes represent the energy content of different interacting parts of the climate system with different heat capacities and response times. Of course, we do not derive this phenomenological model from first principles, but in this paper we test it against observation data. The

model, and the linear approximation, can also be tested against state-of-the-art Earth system models. Work in this direction is in progress. The reality of delayed responses in coupled atmospheric–oceanic GCMs (AOGCMs) has recently been demonstrated by [Geoffroy et al. \(2013\)](#). They fitted the four parameters of the two-box model to runs of 16 different CMIP5 models with step-function forcings, with quite good agreement over 150 yr. For the global response the linearity approximation has been verified in AOGCM simulations (e.g., in [Meehl et al. 2004](#)). We also discuss these points further in the concluding section.

The scaling response model corresponds to replacing  $\mathcal{L}$  by a fractional derivative operator [see [Rypdal \(2012\)](#) for details], which effectively corresponds to replacing the two-box Green’s function with the power-law function

$$G(t) = (t/\mu)^{\beta/2-1} \xi, \tag{9}$$

where  $\mu$  is a scaling factor in the units of time characterizing the strength of the response and  $\xi \equiv 1 \text{ km}^2 \text{ J}^{-1}$  is a factor needed to give  $G(t)$  the right physical dimension.

We shall define our equilibrium reference state such that  $T$  is the temperature relative to the initial temperature  $\hat{T}_0$  in the observed record, that is,  $T = \hat{T} - \hat{T}_0$ , where the hat symbol means that temperature is measured relative to absolute zero (kelvin). The observed record then has  $T(0) = 0$ . This means that we define the “true” forcing  $F(t)$  as the influx relative to the influx that balances the outflux at this initial temperature (the equilibrium influx), and since the system is not necessarily in radiative equilibrium at  $t = 0$ , we generally have that  $F(0) \neq 0$ . Forcing data we use in this paper are given as time series over the time interval  $0 \leq t \leq t_L$  in volcanic  $F_V(t)$ , solar  $F_S(t)$ , and anthropogenic  $F_A(t)$  components with  $F_A(0) = F_S(0) = F_V(0) = 0$ , and hence the total “given” forcing  $F_G = F_V + F_S + F_A$  also has  $F_G(0) = 0$ . Hence the relation between the true forcing and the given forcing data is  $F(t) = F(0) + F_G(t)$ . Since  $F(0)$  is not known a priori it becomes a parameter to be estimated along with other model parameters. According to these conventions the temperature evolution according to Eq. (7) becomes

$$T(t) = \int_{-\infty}^0 G(t-s)F(s) ds + F(0) \int_0^t G(t-s) ds + \int_0^t G(t-s)F_G(s) ds. \tag{10}$$

We note that the initial condition  $T(0) = 0$  implies that

$$T(0) = \int_{-\infty}^0 G(-s)F(s) ds = 0, \tag{11}$$

that is, it puts a restriction on the forcing in the semi-infinite time interval  $-\infty < t < 0$  prior to the recorded period  $0 < t < t_L$ . If we could assume that  $T(t)$  is a stationary stochastic process for  $-\infty < t < 0$ , then this restriction would require that the zero level for  $F(t)$  for  $t < 0$  is chosen such that it has zero mean. If we have more detailed knowledge about the forcing far back in time via paleoreconstructions, this may be a way to determine the zero-level  $F(0)$  for the forcing function that is consistent with a linearization around a radiative equilibrium. If we do not have this information about past forcing, or we do not want to use it, an alternative is to estimate this zero level from the temperature and forcing records we have for  $t > 0$  by treating it as a free model parameter. We will apply both methods in [section 4](#), and demonstrate that they give very similar results. The slightly problematic issue here is the term

$$T_{\text{rnn}}(t) = \int_{-\infty}^0 G(t-s)F(s) ds \tag{12}$$

in Eq. (10), which represents the remnant from all past forcing throughout the time interval  $-\infty < t < 0$  being present in the evolution of  $T(t)$  for  $t > 0$ . If  $G(t)$  is exponential (no LRM), the condition from Eq. (11) implies that this influence vanishes for  $t > 0$ . If  $G(t)$  is scaling with a cutoff at  $t = t_c$ —that is, it has the form

$$G(t) = \xi(t/\mu)^{\beta/2-1} \theta(t-t_c), \tag{13}$$

where  $\theta(t)$  is the unit step function—then the influence of past forcing vanishes for  $t > t_c$ . If such a cutoff does not exist, or  $t_c$  is greater than the length  $t_L$  of the observed temperature and forcing record, then this influence is in principle present over the entire record. This is the nature of long-range memory, and is exactly the property we want to use in predicting future warming for  $t > t_L$  after a period of increasing anthropogenic forcing. However, by choosing the time origin  $t = 0$  to be prior to the recent period of strong anthropogenic forcing, there may have been no strong trends in the evolution of  $F(t)$  through the centuries prior to  $t = 0$  and  $T_{\text{rnn}}(t)$  may be comparatively small for  $t > 0$ . We discuss this issue in detail in [section 4](#).

### 3. Dynamic–stochastic models

In [Rypdal \(2012\)](#) it was shown that the scaling response function gives a somewhat better characterization of the observed record, but no systematic method was presented that would allow rejection of the exponential response hypothesis in favor of the scaling-response hypothesis. The clue to develop such a method is to address the

apparently random fluctuations in the observed record that makes it deviate from the solution to the response model under the prescribed forcing. The forcing given by Hansen et al. (2011) is a deterministic function and the corresponding response should therefore be perceived as a deterministic solution. Even with a correct model of the response the deterministic solution will not be a perfect match to the observed record because the forcing should also have a stochastic component corresponding to the random forcing of the ocean–land heat content from the atmospheric weather systems and stochastic energy flux between the surface ocean layer and the deep ocean resulting from unresolved turbulence. A more complete (dynamic stochastic) model can be constructed by adding a stochastic forcing such that Eq. (7) is generalized to

$$T(t) = \int_{-\infty}^t G(t-s)F(s) ds + \sigma \int_{-\infty}^t G(t-s) dB(s), \quad (14)$$

where Eq. (11) for the deterministic temperature component imposes the restriction

$$\int_{-\infty}^0 G(-s)F(s) ds = 0.$$

Here  $F(t)$  is the deterministic component of the forcing and  $B(t)$  is the Wiener process, sometimes called a Brownian motion. The incremental process  $\sigma dB(t)$  is a Gaussian white-noise measure and is to be perceived as the stochastic forcing. We have introduced an unknown parameter  $\sigma$  representing the strength of this forcing. There are two major advantages of introducing the stochastic forcing:

- (i) Since the observed record in this formulation should be perceived as one realization of a stochastic process produced by the dynamic–stochastic model, the residual difference between this record and the deterministic solution should be perceived as a noise process  $\tilde{T}(t)$  given by the stochastic part of the solution to Eq. (14), that is,

$$\tilde{T}(t) = \sigma \int_{-\infty}^t G(t-s) dB(s). \quad (15)$$

By using the exponential response model, Eq. (15) produces the Ornstein–Uhlenbeck (OU) stochastic process. On time scales less than  $\tau$  this process has the same scaling characteristics as a Brownian motion, that is, the PSD has the power-law form  $P(f) \sim f^{-2}$  for  $f > \tau^{-1}$ . On time scales greater than  $\tau$  the process has the scaling of a white noise and the PSD is flat for  $f < \tau^{-1}$ . This means that if we

analyze a sample of an OU process whose length is much shorter than  $\tau$  we cannot distinguish it from a Brownian motion. On the other hand, if we coarse-grain an OU process in time by averaging over successive time windows of length much greater than  $\tau$ , the resulting discrete-time process is indistinguishable from a white noise. Actually, the PSD has the form of a Lorentzian,  $P(f) \sim [\tau^{-2} + (2\pi f)^2]^{-1}$ . For a discrete-time process the direct analog to the Ornstein–Uhlenbeck process is the first-order autoregressive process AR(1). The scaling response model, on the other hand, produces an fGn for  $-1 < \beta < 1$  and a fractional Brownian motion (fBm) for  $1 < \beta < 3$ . For these noises and motions the PSD for low frequencies has the power-law form  $P(f) \sim f^{-\beta}$ . In principle, an estimator for the PSD (like the periodogram) applied to the observed residual could be compared to the PSD for the two response models to test the validity of the models against each other. In practice, other estimators in this paper will be used, but the idea is the same.

- (ii) Formulating the problem as a parametric stochastic model allows systematic estimation of the parameters  $\{F(0), C, \sigma, \tau\}$  for the exponential model, and  $\{F(0), \mu, \sigma, \beta\}$  for the scale-invariant model. The method is based on maximum-likelihood estimation (MLE), which establishes the most likely parameter set that could produce the observed record from the prescribed forcing. The principles of the MLE employed here are explained in the appendixes.

The significance of the LRM response can be appreciated by looking at Eq. (7) in the Fourier domain,

$$\tilde{T}(f) = \tilde{G}(f)\tilde{F}(f), \quad (16)$$

where  $\tilde{T}$ ,  $\tilde{G}$ ,  $\tilde{F}$  are Fourier transforms of  $T$ ,  $G$ ,  $F$ , and  $\tilde{G}(f)$  is the transfer function of the linear system. This relation naturally leads us to define the frequency-dependent sensitivity as

$$S(f) = |\tilde{G}(f)| = \frac{|\tilde{T}(f)|}{|\tilde{F}(f)|}. \quad (17)$$

For the exponential response model we find

$$S(f) = \frac{1}{C\sqrt{\tau^{-2} + (2\pi f)^2}}, \quad (18)$$

which in the limit  $2\pi f\tau \ll 1$  converges to the equilibrium sensitivity  $S_{\text{eq}} = \tau/C$ . For the scale-invariant model we have

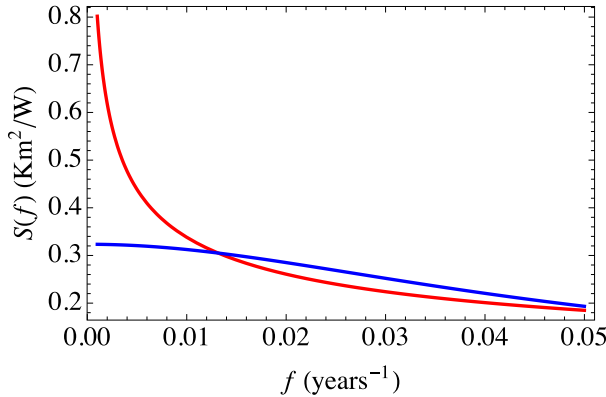


FIG. 3. Frequency-dependent sensitivity  $S(f)$  for the exponential response model (blue) and the scale-invariant model (red) for model parameters given in Table 1.

$$S(f) = \frac{\xi\mu\Gamma(\beta/2)}{|2\pi\mu f|^{\beta/2}}, \quad (19)$$

where  $\Gamma(x)$  is the Euler gamma function. In Fig. 3 we show a plot of  $S(f)$  for the values of the model parameters estimated for the global temperature and forcing record in section 4. Note that the frequency-dependent sensitivities for the two models depart substantially from each other only for frequencies corresponding to time scales longer than a century. Hence it is on these slow time scales that LRM really has serious impact on the

climate dynamics. The dramatic consequences will be apparent when we consider time scales of many centuries in sections 5 through 7.

In principle, the right-hand side of Eq. (17) could be used to estimate  $S(f)$  directly from Fourier transforming the temperature and forcing records, and then to compare with Eqs. (18) and (19) to assess the validity of the two response models. The short length of the records, however, makes the Fourier spectra very noisy, and the ratio between them even more so. Additional complications are that the spiky nature of the forcing record to volcanic eruptions and the unknown amplitude of the stochastic forcing component. Hence, we have to resort to the model parameter estimation described above, and to other estimators than the Fourier transform, to settle this issue.

#### 4. Parameter estimation from instrumental records

The temperature datasets analyzed in this section can be downloaded from the Hadley Center Met Office web site. We consider the global mean surface temperature (GMST) as presented by the Hadley Centre Climatic Research Unit, version 3 (HadCRUT3) monthly mean or annual mean temperatures (Brohan et al. 2006). The forcing record is the one developed by Hansen et al. (2005) and used by Hansen et al. (2011), and is shown in Fig. 4a. The forcings decomposed into volcanic, solar,

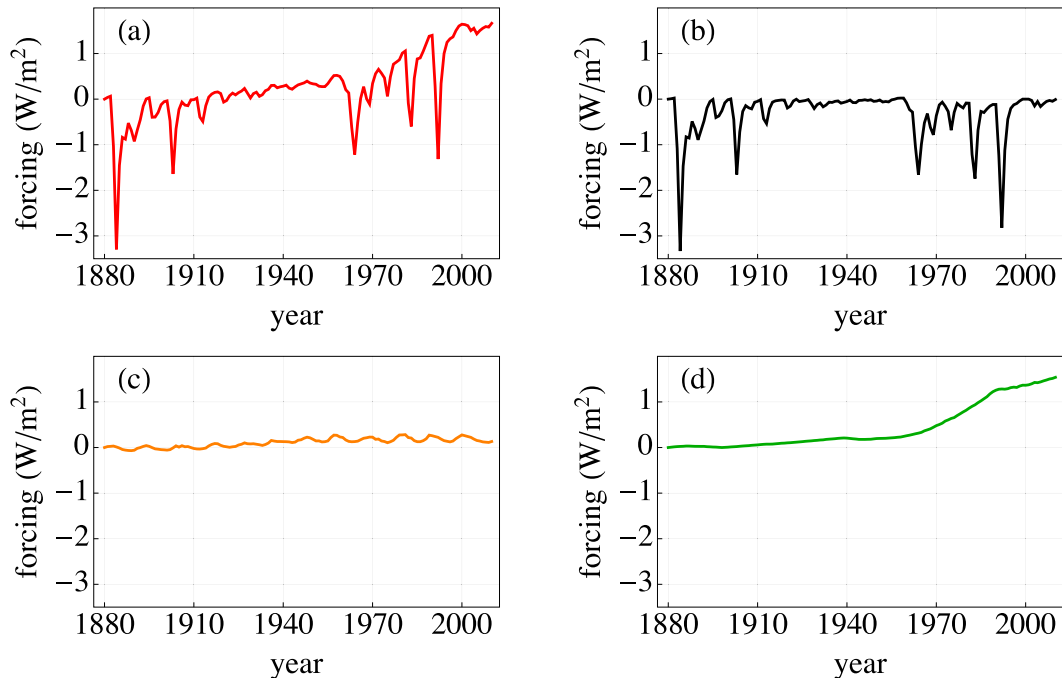


FIG. 4. (a) Total forcing for 1880–2010, (b) volcanic forcing, (c) solar forcing, and (d) anthropogenic forcing.

TABLE 1. The MLE of parameters in the exponential response model and in the scale-free response model. The parameters are estimated from the HadCRUT3 annual temperature record. The parameter  $\sigma_{\bar{T}}$  is defined as the std dev of the stochastic components  $\bar{T}(t)$ . The numbers in the brackets are the mean standard errors obtained from a Monte Carlo study.

Exponential response model	Scale-free response model
$\tau = 4.3 (\pm 0.7)$ yr	$\beta = 0.75 (\pm 0.12)$
$C = 4.2 (\pm 0.2) \times 10^8 \text{ J m}^{-2}$	$\mu = 8.4 (\pm 2.5) \times 10^{-3}$ yr
$F_0 = 0.19 (\pm 0.12) \text{ W m}^{-2}$	$F_0 = 0.19 (\pm 0.16) \text{ W m}^{-2}$
$\sigma_{\bar{T}} = 0.15 (\pm 0.01) \text{ K}$	$\sigma_{\bar{T}} = 0.13 (\pm 0.02) \text{ K}$

and anthropogenic contributions are shown in Figs. 4b–d, respectively. The forcing records go from 1880 until 2010 with annual resolution, so even if the instrumental temperature record goes further back in time and has monthly resolution, the maximum-likelihood estimation of model parameters only employs the 130-yr records with annual resolution. The analysis of the residual noise signal, however, utilizes the monthly resolution to improve the statistics.

The results of the MLE method for the exponential and scaling models are given in Table 1. The heat capacity  $C = 4.2 \times 10^8 \text{ J km}^{-2}$  estimated from the exponential model is very close to that of a 100-m-deep column of seawater, and the time constant 4.3 yr is in the middle of the range (3–5 yr) observed by Held et al. (2010) from instantaneous  $\text{CO}_2$  experiments with the Geophysical Fluid Dynamics Laboratory (GFDL) Climate Model, version 2.1 (CM2.1). What was also observed in those model runs was an additional slower response that showed that equilibrium was not attained after 100 yr of integration, indicating that the exponential model does not contain the whole story. In Fig. 5a we

present the deterministic part of the solutions for both models along with the observed GMST record. Although the solution of the scaling model seems to yield a somewhat better representation of both the multi-decadal variability and the response to volcanic eruptions, the difference between the deterministic solutions of the two models is not striking on these time scales. The reason for this can be understood from Fig. 3. It is on time scales longer than a century that the difference will become apparent. For the stochastic part of the response, however, the two models can be tested against data on all observed time scales. Such a test is performed in Fig. 5b, where the residual noise (the observed GMST with the deterministic solution subtracted) has been analyzed by the DFA technique (Kantelhardt et al. 2001). What is plotted here is the DFA(1) fluctuation function of the residual noise versus time scale. For an AR(1) process (stochastic solution of the exponential model) the slope of this curve in a log–log plot is near 1.5 for time scales much less than  $\tau$ , and near 0.5 for time scales much greater than  $\tau$ , as shown by the blue dashed curve in the figure. For an fGn the slope of the curve is  $(\beta + 1)/2$ , which has been estimated to yield  $\beta \approx 0.75$ , as shown by the red dashed curve. The fluctuation functions of the actual observed residuals with reference to the two models are shown as the blue crosses and the red circles in the figure, showing that the residuals are inconsistent with an AR(1) process, but consistent with an fGn process.

In Fig. 6 we demonstrate that the observed record falls within the uncertainty range of the two dynamic–stochastic models. Here we have generated an ensemble of solutions to the two models with the estimated parameters and plotted the  $2\sigma$  range around the

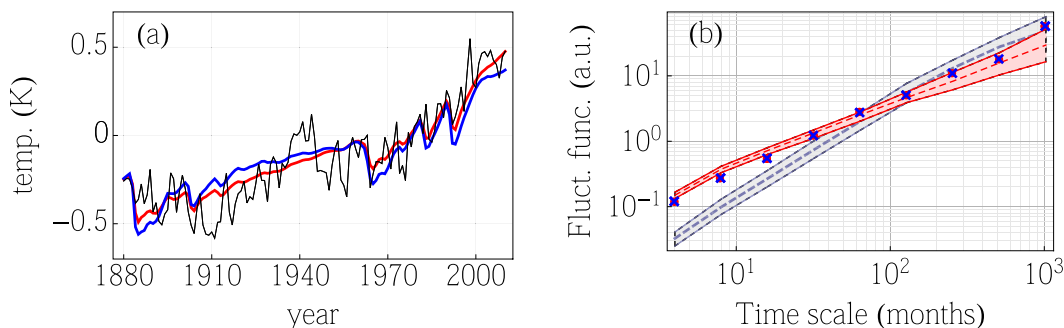


FIG. 5. (a) Deterministic part of the solution where blue indicates the exponential response model, red the scale-invariant response model, and black the HadCRUT3 annual temperature record. (b) Blue crosses denote DFA(1) of monthly GMST record with the deterministic solution of the exponential response model subtracted (the residual). Red circles (obscured because they nearly coincide with the blue crosses) denote the same with the deterministic solution of the scaling model subtracted. Blue dashed curve represents ensemble mean of DFA(1) fluctuation function of simulated AR(1) process with estimated parameters from the exponential response model. Shaded blue area represents 2 times std dev of the distribution of DFA(1) over the ensemble. Red dashed curve and shaded area represent the same for an fGn process with estimated parameters from the scaling model.

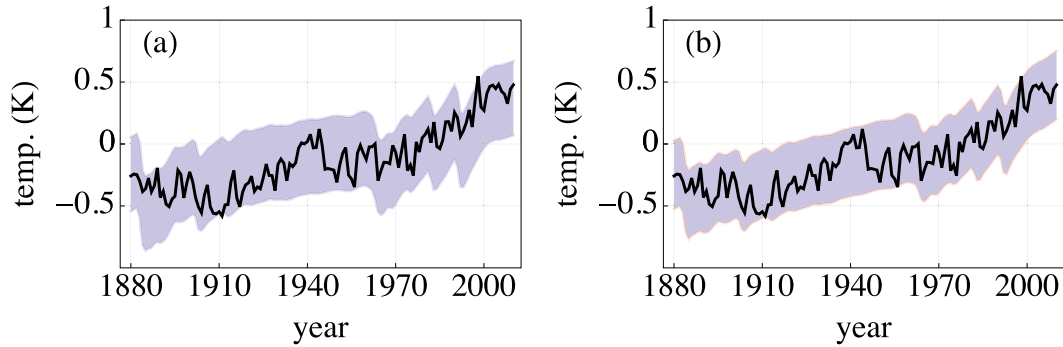


FIG. 6. Black curves are the GMST record and shaded areas are the deterministic part of the solution  $\pm 2$  times std dev of the stochastic part representing the range of solutions to the model for (a) the exponential response model and (b) the scaling response model.

deterministic solutions. The results are shown as the two shaded areas in Figs. 6a and 6b, respectively.

In Fig. 7 we plot the deterministic scaling response to the total forcing along with the separate responses to the volcanic, solar, and anthropogenic forcing components. During the first half of the twentieth century, solar and anthropogenic forcing contribute equally to the global warming trend. After 1950 there is a significant cooling trend resulting from volcanic aerosols, a weaker warming contribution from solar activity, and a dominating anthropogenic warming.

The maximum likelihood estimation employed so far in this section  $\{F(0), C, \sigma, \tau\}$  for the exponential model, and  $\{F(0), \mu, \sigma, \beta\}$  for the scale-free model, using the model Eq. (10), but neglecting the term  $T_{rnn}(t)$ . Hence we have used no information about past forcing. If we use reconstructions of forcing throughout the past millennium (Crowley 2000) we can compute  $F(0)$  from Eq. (11) and  $T_{rnn}(t)$  from Eq. (12) and use the entire Eq. (10), including the term  $T_{rnn}(t)$ , in the computation of  $T(t)$ . In Fig. 8a we plot  $T_{rnn}(t)$  for the period 1880–2080 computed from the reconstruction and the scaling

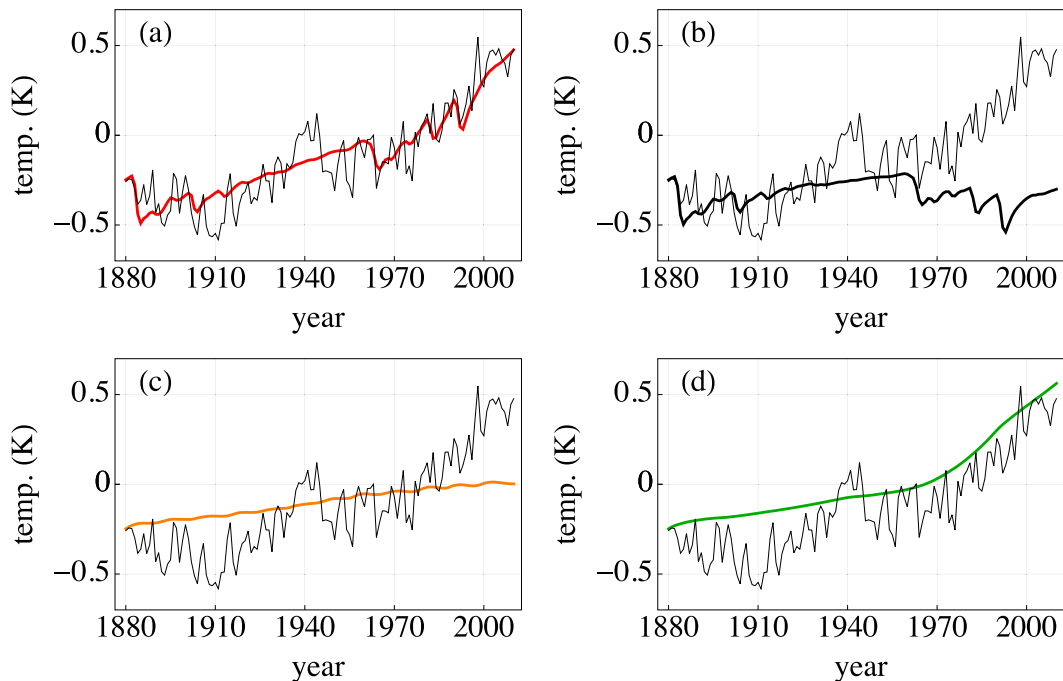


FIG. 7. Deterministic part of forced temperature change for 1880–2010 according to the scale-invariant model from (a) total forcing, (b) volcanic forcing, (c) solar forcing, and (d) anthropogenic forcing. Thin black curves are the GMST record.



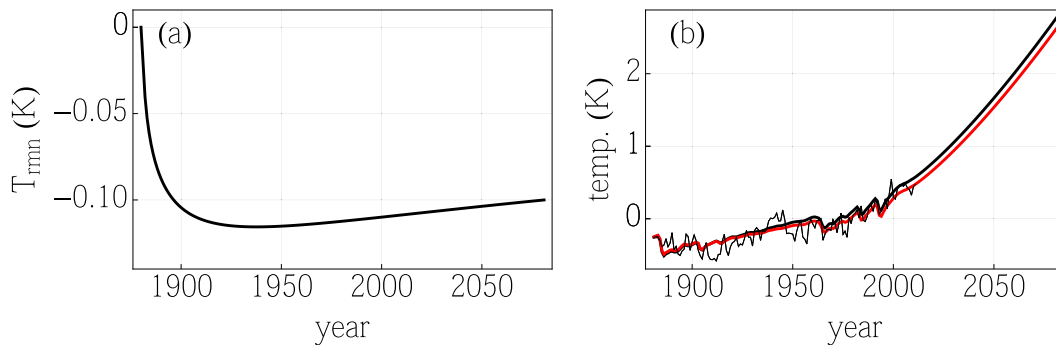


FIG. 8. (a) The remnant from past forcing  $T_{\text{rmn}}$  from 1880 until 2080. (b) Black curve represents the deterministic solution  $T(t)$  including  $T_{\text{rmn}}$  and with  $F(0)$  estimated from forcing data for the period 1000–1880. Red curve represents the deterministic solution estimated by not including  $T_{\text{rmn}}$ , and with  $F(0)$  estimated using forcing data for the period 1880–2010 only. The forcing beyond 2010 used here corresponds to a  $1\% \text{ yr}^{-1}$  increase in atmospheric  $\text{CO}_2$  concentration.

response model with the parameters  $\{\mu, \sigma, \beta\}$  given in Table 1. We observe that this remnant rapidly goes from 0 to approximately  $-0.1 \text{ K}$  because of the forcing imbalance created by the variability over the previous millennium. The rapid initial change is an effect of the finite value of the forcing [ $F = F(0)$ ] around 1880. As  $t$  grows,  $F(t)$  will fluctuate around the zero equilibrium value and eventually be influenced by the rising trend. This terminates the fast change in  $T_{\text{rmn}}(t)$ , which is followed by a slow decay. In Fig. 8b the black smooth curve is  $T(t)$  computed from Eq. (10) and includes  $T_{\text{rmn}}(t)$ . Here,  $F(0)$  is computed from Eq. (11) using reconstructed forcing (Crowley 2000) for the period 1000–1880. The red curve is the same as shown in Fig. 7a, but extended to 2080 using a forcing scenario corresponding to a  $1\% \text{ yr}^{-1}$  increase in atmospheric  $\text{CO}_2$  concentration. Here  $F(0)$  is estimated along with the other model parameters from the instrumental data and  $T_{\text{rmn}}(t)$  is not part of the statistical model from which the parameter  $F(0)$  is estimated. It appears that the two methods yield very similar deterministic solutions for  $T(t)$ , indicating that the (positive) effect of reestimating  $F(0)$  more than compensates the (negative) effect of including  $T_{\text{rmn}}(t)$ . The proximity of the two curves in Fig. 8b shows that the two methods yield very similar results for realistic forcing scenarios for the coming century. For this reason we shall employ the method that does not make use of  $T_{\text{rmn}}(t)$  in the remainder of this paper.

## 5. Predicting reconstructed records

The DFA fluctuation function plotted in Fig. 5b can demonstrate with statistical confidence that the residual is scaling only up to time scales less than  $1/4$  of the length of the 130-yr record (i.e., for 3–4 decades). Verifying LRM on longer time scales requires longer records. This

was done by Rybski et al. (2006) and Rypdal (2012) using detrending techniques like the DFA applied directly to reconstructed temperature records over the last one or two millennia. Here we shall utilize a forcing record for the last millennium (Crowley 2000), shown in Fig. 9, with its decomposition in volcanic, solar, and anthropogenic contributions. Many temperature reconstructions for the Northern Hemisphere exist for this time period [see Rybski et al. (2006) for a selection]. We shall employ our dynamic–stochastic models to the reconstruction by Moberg et al. (2005), which shows a marked temperature difference between the Medieval Warm Period (MWP) and the Little Ice Age (LIA). For the scaling model the parameters estimated from Crowley forcing and Moberg temperature are very close to those estimated from the instrumental records, except for the initial forcing  $F(0)$ . The initial forcing measures how far the climate system is from equilibrium at the beginning of the record, and this will depend on at what time this beginning is chosen. Considering that the timing of volcanic events and the corresponding temperature responses probably are subject to substantial errors in these reconstructions, this might give rise to errors in the parameter estimates. For this reason we have also estimated  $F(0)$  from Crowley forcing and Moberg temperature by retaining the values of the other parameters estimated from the instrumental record and shown in Table 1. The resulting deterministic solutions for the two models are plotted in Fig. 10a, along with the Moberg record. Since only the departures from equilibrium forcing  $F(0)$  are estimated from the reconstruction data, these solutions should be considered as “predictions” of the deterministic component of the forced evolution over the last millennium, based on parameters estimated from the modern instrumental records. The exponential model predicts too low

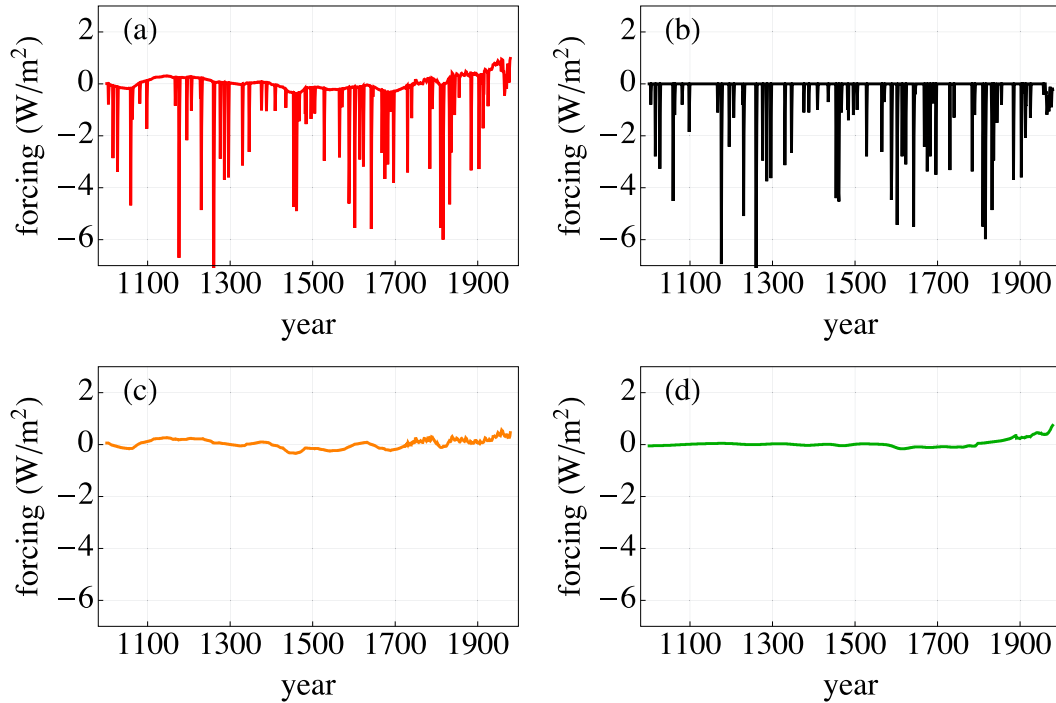


FIG. 9. As in Fig. 4, but for 1000–1978.

temperature in the first half of the record and too strong short-term responses to volcanic eruptions. The scaling model gives a remarkably good reproduction of the large-scale structure of the Moberg record and reasonable short-term volcano responses. The DFA fluctuation functions of the residuals for the two models are plotted in Fig. 10b, and again we observe that the results are consistent with a scaling response over the millennium-long

record and inconsistent with the exponential response model.

Figure 11 shows the scaling response to the total Crowley forcing, along with the responses to the volcanic, solar, and anthropogenic components. The most remarkable feature is that most of the cooling from the MWP to the LIA appears to be caused by volcanic cooling and not by the negative solar forcing associated

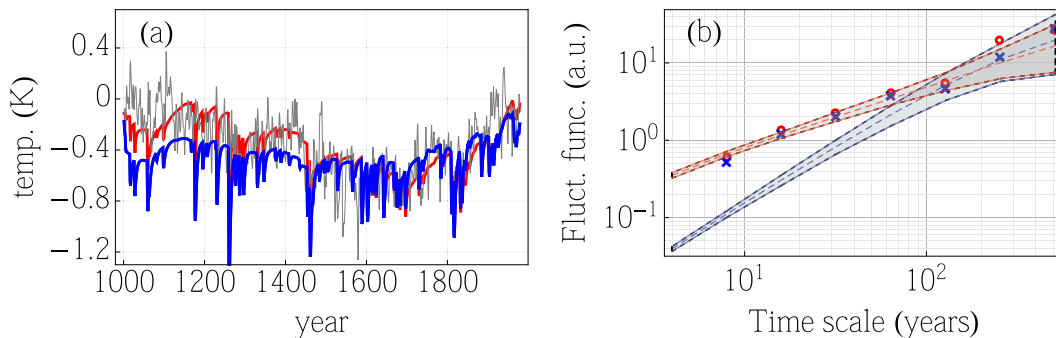


FIG. 10. (a) Deterministic part of the solution with Crowley forcing where blue indicates the exponential response model, red the scaling response model, and black the Moberg annual temperature reconstruction record. (b) Blue crosses denote DFA(1) of Moberg record with the deterministic solution of exponential response model subtracted. Red circles denote the same with the deterministic solution of scaling model subtracted (residual). Blue dashed curve represents ensemble mean of DFA(1) fluctuation function of simulated AR(1) process with estimated parameters from the exponential response model. Shaded blue area represents 2 times std dev of the distribution of DFA(1) over the ensemble. Red dashed curve and shaded area represent the same for an fGn process with estimated parameters from the scaling model.

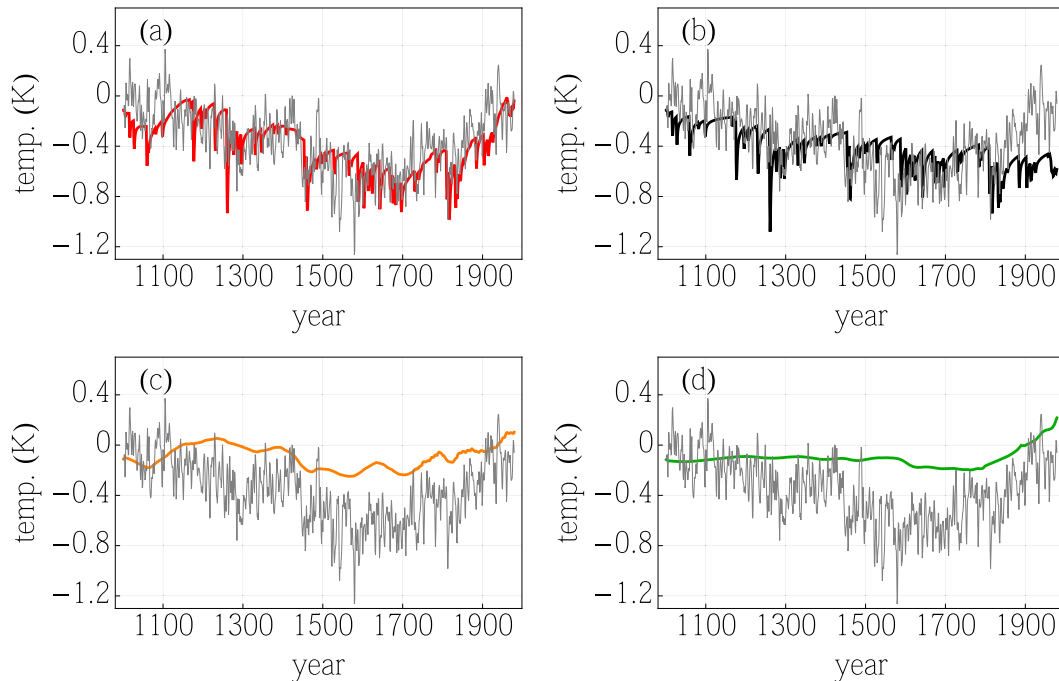


FIG. 11. Deterministic part of forced temperature change for 1000–1978 according to the scaling model with  $F(0)$  estimated from the Moberg record and  $\{\beta, \mu, \sigma\}$  from the instrumental record. Gray curve is the Moberg record and results are shown from (a) total forcing, (b) volcanic forcing, (c) solar forcing, and (d) anthropogenic forcing.

with the Maunder Minimum, in agreement with recent findings by Schurer et al. (2014). On the other hand, the solar contribution to the warming from the LIA until the mid-twentieth century is comparable to the anthropogenic. After this time the warming is completely dominated by anthropogenic forcing, in agreement with what was shown in Fig. 7.

## 6. Truncated long-range memory

Does long-range memory imply that we still feel the effect of long past volcanic explosions like the Tambora (1815) eruption? Let us examine this question, which is frequently asked in discussions about LRM in the climate response. On centennial time scales this volcanic eruption represents a delta function forcing  $\delta F(t) = \delta_{t,t_1}$ , and hence the response decays like  $\delta T(t) = [(t - t_1)/\mu]^{\beta/2-1}\xi$ . The parameters presented in Table 1 are computed from time series with annual resolution, so  $\delta T = (1/\mu)^{\beta/2-1}\xi$  is to be considered as the instantaneous response manifested by the temperature change recorded the year after the eruption. Thus, after 200 yr this response is reduced by a factor  $200^{\beta/2-1} \sim 0.04$ , assuming  $\beta \approx 0.75$  as estimated in Table 1. Using the value of  $\mu$  given in Table 1 or looking at Fig. 11a, we find that the instantaneous response is about 0.5 K, so the remnant after 200 yr is around 0.02 K. This is much

less than the stochastic climate noise, which was estimated in Table 1 to be  $\sigma_{\bar{T}} = 0.13 (\pm 0.02)$  K, and means that the effect of Tambora cannot be detected in today's temperature data. These considerations illustrate that the effect of LRM is not very important for the long-term impact of single eruptions or fast oscillations, but the delayed impact of trends or monotonic shifts in the forcing, including shifts in the frequency or strength of episodic events such as volcanic eruptions, may be considerable. One must not forget, however, that the scale-invariant response is an idealized toy model designed to incorporate slowly components of the climate system into one single response function. One must also keep in mind that the climate system is highly nonlinear, and that the linear expansion around a radiative equilibrium is inadequate if the system evolves far from the initial quasi-equilibrium state. With forcing scenarios that shift the level of forcing semipermanently to a new level, the linear LRM temperature response will continue to grow indefinitely like  $t^{\beta/2-1}$ . Such a growth will of course eventually be saturated by nonlinear effects, in the same manner as they will saturate linear instabilities in any realistically modeled dynamical system. Hence our linear, scaling response theory exhibits the same strengths and limitations as linear stability theory, and there is of course a need to examine these limitations. One simple way to model the

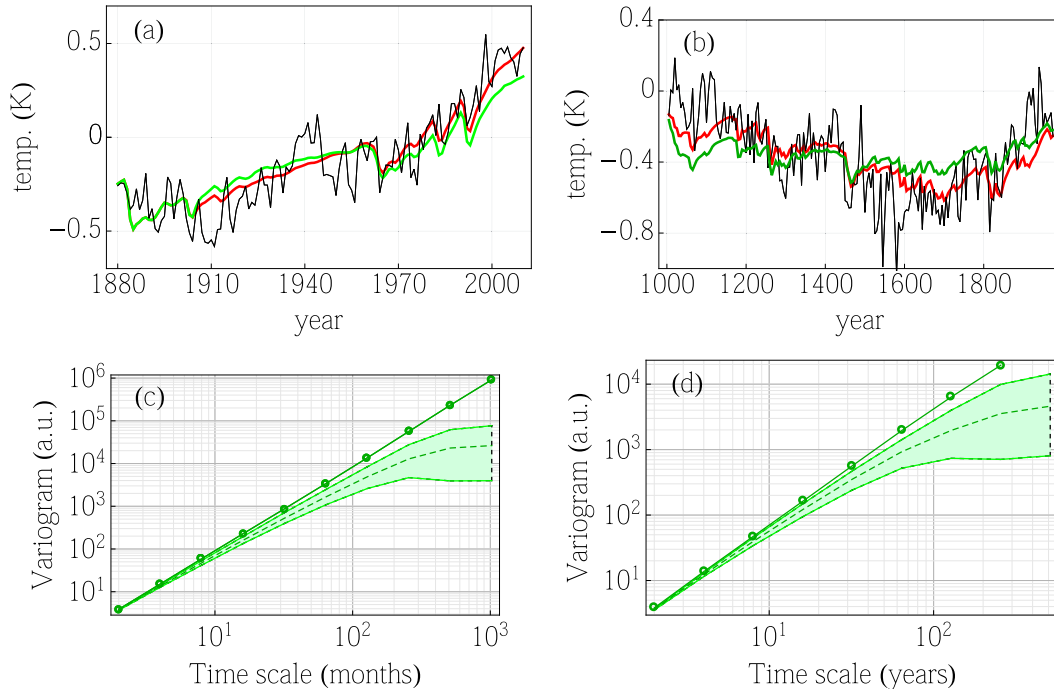


FIG. 12. (a) Deterministic solution corresponding to the instrumental temperature record with a truncated scaling response function with cut-off time  $t_c = 10$  yr (green curve), alongside the solution for the untruncated response (red curve). (b) As in (a), but for the reconstructed record with  $t_c = 100$  yr. (c) Variogram of the residual obtained by subtracting the deterministic solution from the observed instrumental temperature record (dots). The green dashed line is the ensemble mean of variograms of realizations of a simulated stochastic process generated by Eq. (15) with a power-law kernel truncated at  $t_c = 10$  yr. The green shaded area indicates 95% confidence for the variogram estimate. (d) As in (c), but for the reconstructed record with  $t_c = 100$  yr.

effect of nonlinear saturation of the LRM response is to investigate the effect a truncation of the scale-free response function as suggested in Eq. (13).

In Fig. 12a we have plotted the deterministic solution corresponding to the instrumental temperature record with a truncated scaling response function with cutoff time  $t_c = 10$  yr (green curve), alongside the solution for the untruncated response (red curve). The difference between the two solutions is not remarkable and cannot be used as model selection criterion. In Fig. 12c, however, we have plotted a variogram (log–log plot of the second-order structure function) of the residual obtained by subtracting the deterministic solution from the observed temperature record (dotted line). The result is consistent with an fGn process scaling on time scales up to  $10^2$  yr, which was also shown in Fig. 5b [using the DFA (1) fluctuation function]. The dashed line surrounded by the green field is the ensemble mean of variograms of realizations of a simulated stochastic process generated by Eq. (15) with a truncated power-law kernel. The green field indicates 95% confidence for the variogram estimate. It is seen that the scaling properties of the actual residual noise is not captured by the truncated

model if we choose  $t_c$  as small as 10 yr. By increasing  $t_c$  beyond approximately 30 yr we cannot reject the truncated model based on the instrumental data, but the same study can be made on the data from the millennium reconstructions, and some results are shown in Fig. 12c. Here we observe that the truncated model with  $t_c = 100$  yr gives a deterministic solution that gives a considerably poorer fit to the observed record than the full scale-free model, and again the variogram of the noise generated by the truncated model is inconsistent with that obtained from the real residue. We conclude from this that the cutoff time  $t_c$  in the scale-free response is not less than a century, and hence that predictions made for the twenty-first century based on the scale-free model are supported by the forcing and temperature data available.

## 7. Perspectives on climate sensitivity

For predictions of future climate change on century time scales the equilibrium climate sensitivity may not be the most interesting concept. The frequency-dependent climate sensitivity  $S(f)$  given by Eq. (17) is more relevant.

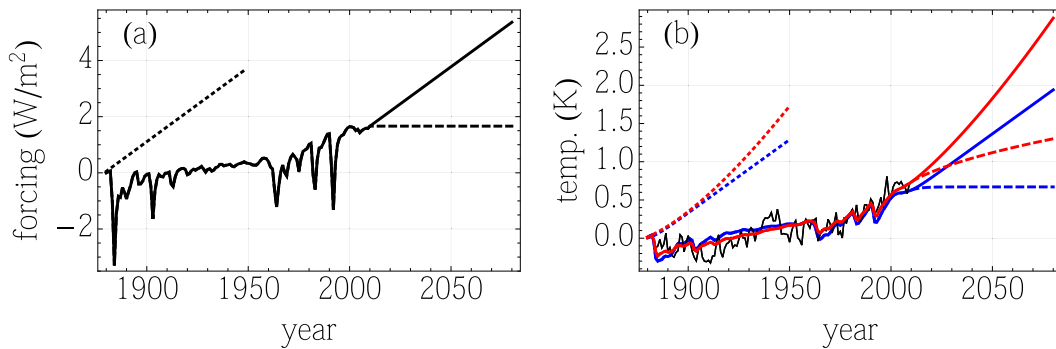


FIG. 13. (a) Dotted line is the forcing scenario corresponding to  $1\% \text{ yr}^{-1}$  increase in  $\text{CO}_2$  concentration starting in 1880. Solid curve is the historical forcing for 1880–2010 followed by  $1\% \text{ yr}^{-1}$  increase in  $\text{CO}_2$  concentration after 2010. Dashed line after 2010 is forcing kept constant at the 2010 level. (b) GMST evolution according to the two response models with parameters given in Table 1 for the three forcing scenarios described for (a). Blue curves indicate the exponential response model and red curves the scaling response model.

The transient climate response (TCR), defined as the temperature increase  $\Delta T_{\text{tr}}$  at the time of doubling of  $\text{CO}_2$  concentration in a scenario where  $\text{CO}_2$  concentration increases by  $1\% \text{ yr}^{-1}$  from preindustrial levels, can also readily be computed from the response models. In Fig. 13a this forcing is shown as the dotted curve to the left (the forcing is logarithmic in the  $\text{CO}_2$  concentration, so the curve is linear). The response curves to this forcing according to the two response models are shown as the blue and red dotted curves to the left in Fig. 13b. At the end of these curves (the time of  $\text{CO}_2$  doubling after 70 yr) the temperatures represent the respective TCRs. They are both in the lower end of the range presented by Solomon et al. (2007). A more useful definition is to consider the response to the same  $\text{CO}_2$  increase from the present climate state that is established from the historical forcing since preindustrial times. This response is what is shown as the blue and red full curves in Fig. 13b for the next 70 yr. For the scale-free model the temperature in year 2010 lags behind the forcing because of the memory effects, and the energy flux imbalance  $dQ/dt$  established by the historical evolution at this time gives rise to a faster growth in the temperature during the next 70 yr, compared to the  $\text{CO}_2$  doubling scenario starting in year 1880. The value of  $\Delta T_{\text{tr}}$  (according to the modified definition) is 1.3 K in the exponential response model, but 2.1 K for the scale-invariant model. The latter is very close to the median for the TCR given in Solomon et al. (2007). Another illustration of the memory effect can be seen from the forcing scenario where the forcing is kept constant after 2010 as shown by the dashed line in Fig. 13a. The corresponding responses are given by the blue and red dashed curves in Fig. 13b. The short time constant in the exponential model makes the temperature stabilize in equilibrium after a few years, while in the scale-free model the temperature

keeps rising as  $[2\mu^{1-\beta/2}F(2010)/\beta](t-2010)^{\beta/2}$  for  $t > 2010$  yr. As discussed in section 6 this monotonic rise in the temperature will not continue indefinitely, and will stabilize for  $t - 2010 > t_c$  in a more realistic truncated LRM model. But since our analysis in section 6 indicates that an effective  $t_c$  is greater than a century, the scaling model is adequate for the time scale scales shown in Fig. 13.

In a recent paper Aldrin et al. (2012) supplemented the information in the time series of total forcing and temperatures of the Northern and Southern Hemisphere with a series for the evolution of total ocean heat content (OHC) through the last six decades. Their response model is a simple deterministic energy-balance climate/upwelling diffusion ocean model augmented by a first-order autoregressive stochastic process for the residual. The equilibrium climate sensitivity is a parameter in the deterministic model, and since the stochastic term for the residue is AR(1) the full model cannot reproduce the LRM properties of the observed climate signal. The purpose of the work is to produce more accurate estimates of  $S_{\text{eq}}$ , and the introduction of the OHC data is a new observational constraint on this estimate. We find it interesting to consider these data in the light of a slightly rewritten version of the energy-balance equation Eq. (2):

$$Q'(t) = -\frac{\tilde{T}(t)}{S(t)} + F(0) + \tilde{F}(t), \quad (20)$$

where  $Q' \equiv dQ/dt$ ,  $S(t)$  can be thought of as a time-dependent climate sensitivity,  $\tilde{T}(t)$  is the perturbation of the temperature relative to the temperature at time  $t = 0$ ,  $\tilde{F}(t)$  is the perturbation of the forcing relative to the forcing at  $t = 0$  [i.e.,  $\tilde{T}(0) = \tilde{F}(0) = 0$ ], and  $F(0)$  is the radiative forcing imbalance at  $t = 0$ . From this follows the obvious relation

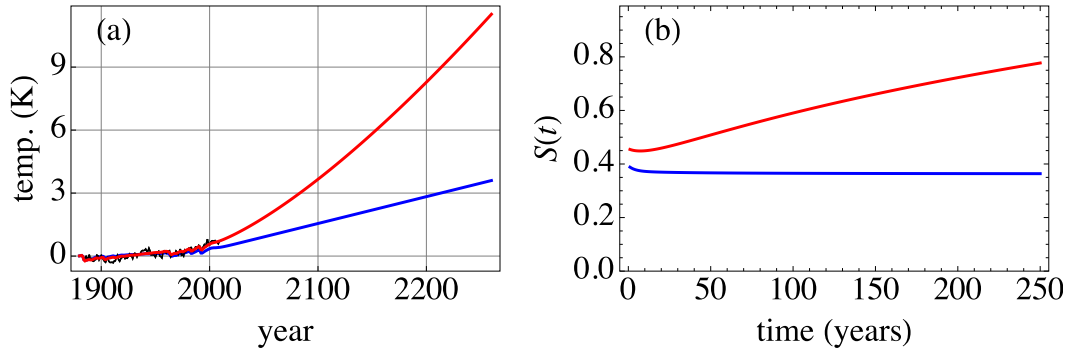


FIG. 14. (a) Global temperature evolution in response to the  $1\% \text{ yr}^{-1}$   $\text{CO}_2$  increase forcing scenario, starting in year 2010. (b) Evolution of the time-dependent climate sensitivity  $S(t)$  in response to this forcing scenario assuming a linear increase in OHC corresponding to a net positive energy flux of  $0.25 \text{ W m}^{-2}$ . The time origin  $t = 0$  is year 2010. Blue curves indicate the exponential response model and red curves the scaling model.

$$Q'(0) = F(0), \quad (21)$$

which allows us to rewrite Eq. (20) in the form

$$S(t) = \frac{\tilde{T}(t)}{\tilde{F}(t) + Q'(0) - Q'(t)}. \quad (22)$$

From the observation data used in Aldrin et al. (2012) we could make crude linear trend approximations of OHC, total forcing, and global temperature:  $Q'(t) = Q'(0)$ ,  $\tilde{F}(t) \approx 0.03t \text{ W m}^{-2}$ , and  $\tilde{T}(t) \approx 0.015t \text{ K}$ , where  $t$  is time after 1950 in units of years. Hence we have the approximate expression for the climate sensitivity,

$$S(t) = \frac{\tilde{T}(t)}{\tilde{F}(t)} \approx 0.5 \text{ K m}^2 \text{ W}^{-1}. \quad (23)$$

Hence these crude trend estimates over the last six decades yield results consistent with the existence of an equilibrium climate sensitivity very close to the best estimate of Aldrin et al. (2012). If we suppose, on the other hand, that the linear trend approximation in temperature is not quite correct, the picture may be different. Consider a linearly increasing forcing as in the future  $1\% \text{ CO}_2$  increase scenario shown by the full curve in Fig. 13a, but assume that the temperature evolves according to the scaling response to this forcing shown by the red full curve in Figs. 13b and 14a. By inserting these data into Eq. (23) we obtain the time-varying climate sensitivity shown in Fig. 14b (here the time origin is chosen in year 2010). Using the temperature evolution for the exponential response shown by the blue curves in Figs. 13b and 14a yields the nearly constant climate sensitivity given by the blue curve in Fig. 14b. This demonstrates that the temperature may increase according to the power law  $\sim t^{\beta/2+1}$  under a linearly increasing forcing and a linearly increasing

OHC, provided stronger positive feedback mechanisms take effect on longer time scales and raise the climate sensitivity. In fact, this idea is just a time-domain statement of the concept of a frequency-dependent sensitivity that was formulated in section 3. The scenario of  $1\% \text{ yr}^{-1}$  increase in  $\text{CO}_2$  concentration continued 250 years into the future is a very extreme one, and corresponds to a raise in concentration of more than one order of magnitude. However, our results show that within the framework of the scaling model, a scenario where the global temperature increases by more than  $10 \text{ K}$  while the OHC maintains a positive linear growth rate, is consistent with only a moderate increase in  $S(t)$  from  $0.5$  to  $0.8$ . One important message from these considerations is that the introduction of a moderately variable time-dependent climate sensitivity will make the scale-invariant LRM response on time scales up to several centuries consistent with energy balance considerations.

## 8. Discussion and conclusions

We have in this paper considered linear models of global temperature response and maximum-likelihood estimation of model parameters. The parameter estimation is based on observed climate and forcing records and an assumption of additional stochastic forcing. This modeling shows that a scale-invariant response is consistent with the stochastic properties of the noisy components of the data, whereas an exponential model is not. This observation disagrees with Mann (2011), who contends that the purely stochastic solution to the exponential response model [an AR(1) process] is consistent with the global instrumental record. The basic weakness in Mann's paper is uncritical application of built-in routines for estimation of the memory exponent

on time series that do not exhibit scaling properties [such as the AR(1) process]. When the scaling properties are tested, as we do in Fig. 5b, the residuals of the observed and exponentially modeled record are clearly distinguishable. Mann argues that no “exotic physics” is necessary to explain the persistence observed in the global records. Our analysis, however, shows that the exponential response model is insufficient to explain the observed scaling properties. But the physics needed to explain these delayed responses is not particularly exotic, as it may be sufficient to take into account the interactions between the ocean mixed layer and the deep ocean that are observed in AOGCM simulations (Held et al. 2010; Geoffroy et al. 2013).

The scaling model with parameters estimated from the modern instrumental temperature and forcing record successfully predicts the large-scale evolution of the Moberg reconstructed temperature record when the Crowley forcing for the last millennium is used as input. Solutions for the volcanic, solar, and anthropogenic components of the Crowley forcing show that the model ascribes most of the temperature decrease from the MWP to the LIA to the volcanic component, while the rise from the LIA to year 1979 is attributed to both solar and anthropogenic forcing up until about year 1950 and primarily to anthropogenic forcing after this time.

The temperature of the planetary surface (whose most important component is the ocean mixed layer) is driven by radiative forcing and energy exchange with atmosphere and deep ocean, some of which can be modeled as stochastic. Even when the mean energy flux to the surface layer is constant in time the total energy content of the system may vary, and if this variability is large on time scales beyond a century it may have little meaning to operate with the notion of an equilibrium climate sensitivity. Thus, the long-range dependence in the climate response implies that the equilibrium climate sensitivity concept needs to be generalized to encompass a time scale–dependent sensitivity that incorporates the effect of increasingly delayed positive feedbacks. This may have far-reaching implications for our assessment of future global warming under strong anthropogenic forcing sustained over centuries, as illustrated by the difference between the projected warming according to the scaling and exponential response models shown in Fig. 14a.

The great advantage of the response model approach is that it eliminates the influence of correlation structure of the forcing in the temperature signal, and reveals the memory structure of the climate response. It reveals a clean scaling of the residual temperature signal that is maintained at least up to the scales that can be analyzed with reasonable statistics in the millennium-long record, which is a few hundred years.

The importance of the “background” continuum of time scales in climate variability has been stressed by Lovejoy and Schertzer (2013). In a short review of their own work, Lovejoy (2013) shows results based on application of their Haar structure function technique to reanalysis, instrumental, and multiproxy temperature records. For twentieth-century reanalysis local records (75°N, 100°W) they find very weak persistence ( $\beta \approx 0$ ) but a transition to  $\beta \approx 1.8$  on longer time scales. For instrumental global records they find a spectral plateau of  $\beta \approx 0.8$  on time scales up to a decade but the same transition to  $\beta \approx 1.8$  on longer time scales. For the multiproxy NH records they find  $\beta \approx 0.8$  and here the transition appears after 5–10 decades. By similar analysis of ice core data they also obtain  $\beta \approx 1.8$  on the longer time scales, and argue that this transition constitutes the separation between a “macroweather” regime and a “climate” regime. The analysis presented here does not support that such a transition in the scaling properties of internal variability takes place on decadal time scales in global or hemispheric records. These scaling properties are shown by the DFA fluctuation functions of the residuals in Figs. 5b and 10b, and indicate  $\beta \approx 0.8$  scaling throughout the instrumental century-long record and at least up to several centuries scale in the millennium-long multiproxy record, respectively. The transition on multidecadal time scale also fails to show up in the detrended scaling analysis of proxy data in Rybski et al. (2006) and Rypdal et al. (2013). We suggest that the transition in global (NH) multiproxy data reported by Lovejoy (2013) is a consequence of not distinguishing between forced and stochastic response (alternatively, by not properly eliminating “trends” imposed by external forcing). A transition to a more persistent climate regime may perhaps be identified on millennium time scales, but it is an open and interesting question whether the rise of  $\beta$  from a stationary ( $\beta < 1$ ) to a nonstationary regime ( $\beta > 1$ ) is an actual change in the properties of the climate response or an effect of trends imposed by orbital forcing. However, the transition in scaling of local records from  $\beta \approx 0$  to larger  $\beta$  seems to reflect internal dynamics, since local records exhibit (at least over land) very low persistence up to the scales of a few decades that we can reliably estimate from the reanalysis data. Further analysis by application of the response model to local data may help to identify the scale at which this transition in scaling of internal dynamics takes place. Such a transition will naturally take place at the scales where global, purely temporal fluctuations start to dominate over spatiotemporal fluctuations in the local records. For time scales longer than the weather regime, such spatiotemporal fluctuations are associated with the interannual, decadal, and

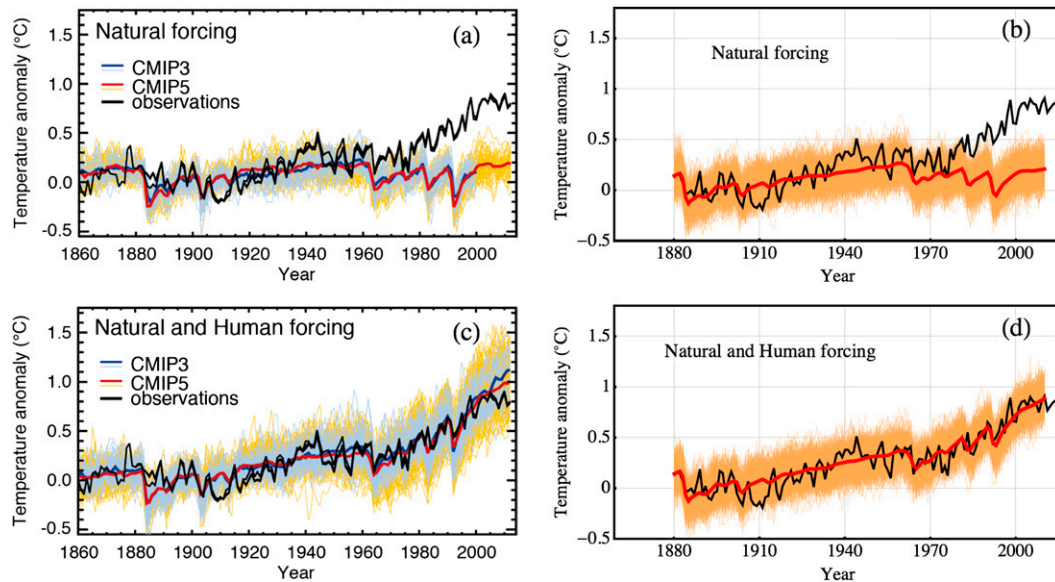


FIG. 15. (a) Individual runs and ensemble means of the CMIP3 and CMIP5 ensembles with natural forcing only. The black curves are global instrumental temperature records. (c) As in (a), but with natural and human forcing. (b),(d) As in (a),(c), but for ensembles of realizations of the LRM response model. The black curves represent the HadCrut4 instrumental record. Adapted from [Stocker et al. \(2013\)](#), FAQ 10.1, their Fig. 1.

multidecadal modes of the climate system, and hence we would expect that this transition scale exceeds all the characteristic time scales of these modes.

In some recent papers multiple regression models have been constructed to assess the relative influence of volcanic, solar, and anthropogenic forcing components, in addition to the ENSO signal. These have been used to demonstrate that the post-2000 hiatus in global warming disappears after the natural forcing and the ENSO signal have been eliminated, and leaves an essentially linear anthropogenic trend over the last few decades ([Foster and Rahmstorf 2011](#)). Such methods have also been used for prediction ([Lean and Rind 2009](#)). The problem with this kind of statistical modeling is that the models contain a large number of fitting parameters with a considerable risk of overfitting, and that they lack any physical principle that allows reduction of this number of free parameters. For instance, the weight of different forcing components and the delay time for the response to each of them are left as free fitting parameters, while in the real world these parameters are determined by physics that is to great extent known. Our approach is also statistical, but it is constrained by the physical idea of a linear response function of a particular form. We use weights between force components that are known, and we assume that the response function (and hence the response time) to different forcings is the same. The parameters that are left to be estimated statistically are only those that are not well known from physical modeling. In the LRM response model there are only two parameters that characterize the

response ( $\mu$  and  $\beta$ ). In the two-box model there are four parameters ([Geoffroy et al. 2013](#)). This means that the risk of overfitting is substantially reduced in the LRM model. Yet a comparative evaluation of these two models against AOGCM experiments should be done.

The deterministic response could be tested against multimodel ensemble means with specified forcings. Such means and the individual runs can be found for instance in frequently asked questions (FAQ) section 10.1, Fig. 1 in [Stocker et al. \(2013\)](#), for the ensembles from phases 3 and 5 of the Coupled Model Intercomparison Project (CMIP3 and CMIP5). The part of this figure that shows the global temperature evolution for those ensembles for natural and natural plus human forcing are shown in [Figs. 15a and 15c](#). The corresponding response model results are shown in [Figs. 15b and 15d](#). There are striking similarities as well as some interesting differences between the multimodel ensembles and the response model ensembles. The overall shapes of the mean response (which in the response model is equivalent to the deterministic response) are very similar, and so are the overall variances in the two ensembles. The response model gives a more accurate description of the observed volcanic responses and the observed hiatus over the last decade, which suggests that the climate models to some extent underestimate the strength of the long-range response. Neither model ensemble means capture quite the observed hiatus, and the reason for this seems to be the importance of the strong El Niño event of 1998, which makes the temperature curve in the following decade appear more flat. Such an event is



unpredictable in both model classes, but can appear by chance both in individual climate model runs and in realizations of the stochastic model. Hence, the hiatus appears well within the error bars of both model classes and gives no indication that global warming has come to a halt.

The large scatter of the individual climate model runs relative to the ensemble means is described in the stochastic response model as the response to the stochastic forcing. In Figs. 5 and 10 we have analyzed this scatter (the residual) in the observed and reconstructed surface temperature, respectively, and found that they are well described as a persistent fractional Gaussian noise. In a recent paper (Østvand et al. 2014) we have investigated the LRM properties of the global surface temperature in a number of millennium-long climate model simulations. We consistently find persistent LRM scaling in these models, both with historical forcing and in control runs. Hence, the statistics of the internal variability of global temperature as appearing as scatter in model ensembles is well described by the stochastic response model, even though the stochastic forcing term has not been derived from first principles.

*Acknowledgments.* This work has received support from the Norwegian Research Council under Contract 229754/E10, from the Tromsø Research Foundation, and from COST action ES1005 (TOSCA). The authors acknowledge useful discussions with Ola Løvstletten.

## APPENDIX A

### Response Functions and Fractional Gaussian Noise

Processes defined by stochastic integrals on the form  $\int_{-\infty}^t G(t-s) dB(s)$  are by construction zero-mean and Gaussian. However, using the Itô isometry (Øksendal 2003), one observes that the process defined by Eq. (1) is not well defined since the variances  $E[X(t)^2]$  are infinite. For instance,

$$\begin{aligned} E[X(0)^2] &= \int_{-\infty}^0 G(-s)^2 ds \\ &= \int_{-\infty}^0 (-s)^{\beta-2} ds = +\infty. \end{aligned} \quad (\text{A1})$$

For  $\beta \in (1, 3)$ , the divergence of the integral in Eq. (A1) is due to the heavy tail of the Green's function  $G(t) = t^{\beta/2-1}$ , and in this case the problem can be resolved by modifying the construction so that  $X(0) = 0$ . The modified construction

$$\begin{aligned} X(t) &= \int_0^\infty (t-s)^{\beta/2-1} dB(s) \\ &+ \int_{-\infty}^0 \{(t-s)^{\beta/2-1} - (-s)^{\beta/2-1}\} dB(s) \end{aligned} \quad (\text{A2})$$

is identical to representation of fBm of Mandelbrot and van Ness (1968). For  $\beta \in (-1, 1)$  however, the integral in Eq. (A1) diverges because of the singularity at  $t = 0$  of the Green's function, a problem that is not resolved by the modification in Eq. (A2).

As with white noise, fGn cannot be defined as a traditional-type stochastic process in continuous time, but rather as a random signed measure. Just as the white noise measure  $dB(t)$  defines a Brownian motion via integration, the fGn integrates to fractional Brownian motion. In fact, if one accepts Eq. (A2) as a formal expression, then performing the integral  $\int_0^t X(t') dt'$  and interchanging the order of integration yields

$$\begin{aligned} \int_0^t X(t') dt' &= \frac{\beta}{2} \int_0^\infty (t-s)^{\beta/2} dB(s) \\ &\times \frac{\beta}{2} \int_{-\infty}^0 \{(t-s)^{\beta/2} - (-s)^{\beta/2}\} dB(s), \end{aligned} \quad (\text{A3})$$

which is an fBm with self-similarity exponent  $h = (\beta + 1)/2$ . This process is proportional to the standard  $h$ -self-similar fBm  $B_h(t)$ , which is defined as the zero-mean Gaussian process with covariance  $E[B_h(t)B_h(s)] = (t^{2h} + s^{2h} - |t-s|^{2h})/2$ . A well-defined version of Eq. (14) can therefore be formulated as the integral equation

$$\begin{aligned} \int_0^t T(t') dt' \\ = \int_0^t \int_{-\infty}^t G(t-s)F(s) ds dt' + \sigma \mu^{-(\beta+1)/2} B_{(\beta+1)/2}(t). \end{aligned} \quad (\text{A4})$$

Discretizations of Eq. (A4) are of the form

$$\mathbf{T} = \mathbf{GF} + \mathbf{x}, \quad (\text{A5})$$

where  $\mathbf{T} = (T_1, T_2, \dots, T_n)^T$  (superscript T denotes transpose) is the random vector representing the temperature record and  $\mathbf{F} = (F(0) + F_1, \dots, F(0) + F_n)^T$  is the deterministic component of the forcing [with  $F(0)$  as a free parameter], that is,  $T_i = T(i\Delta t)$  and  $F_i = F(i\Delta t)$ , where  $\Delta t$  is the time resolution of the records. The matrix  $\mathbf{G}$  is defined from the Green's function by  $G_{ij} = G[(i-j)\Delta t]$ , and the vector  $\mathbf{x} = (x_1, \dots, x_n)^T$  is a discrete-time fGn, that is, a Gaussian random vector with zero mean and covariance,

$$E[x_i x_j] = \frac{\sigma_T^2}{2} \{ (|i-j|+1)^{\beta+1} - 2|i-j|^{\beta+1} + (|i-j|-1)^{\beta+1} \},$$

with  $\sigma_T^2 = (\Delta t/\mu)^{\beta+1} \sigma^2$ .

## APPENDIX B

### Maximum-Likelihood Estimation

In discretized versions the dynamic–stochastic models defined by Eqs. (14) and (A4) can be written as Eq. (A5). For the exponential response model  $\mathbf{x}$  is an AR(1) process

$$x_{k+1} = ax_k + \phi \varepsilon_k,$$

where  $\phi = \sigma/C$ ,  $a = 1 - 1/\tau$ , and  $\varepsilon_k$  are independent and identically distributed (i.i.d.) Gaussian variables of unit variance. In the scale-free model the process  $\mathbf{x}$  is an fGn. To emphasize the parameter dependence we denote the AR(1) process by  $\mathbf{x}_{C,\sigma,\tau}$  and the fGn by  $\mathbf{x}_{\mu,\sigma,\beta}$ . In the same way we denote the Green's function by  $G_{C,\tau}$  in the exponential response model, and by  $G_{\mu,\beta}$  in the scale-free response model.

By a simple change of variables the  $n$ -dimensional probability density function (pdf) of the random vector  $\mathbf{T}$  is related to the pdf of  $\mathbf{x}$  through

$$p_{\mathbf{T}}(\mathbf{T}) = p_{\mathbf{x}}(\mathbf{T} - \mathbf{GF}).$$

For temperature observations  $\mathbf{T}$  the likelihood function for the exponential response model becomes

$$L\{C, \sigma, \tau, F(0)\} = p_{\mathbf{x}_{C,\sigma,\tau}}(\mathbf{T} - G_{C,\tau}\mathbf{F}), \quad (\text{B1})$$

and for the scale-free response model:

$$L\{\mu, \sigma, \beta, F(0)\} = p_{\mathbf{x}_{\mu,\sigma,\beta}}(\mathbf{T} - G_{\mu,\beta}\mathbf{F}). \quad (\text{B2})$$

We see that computation of these likelihoods essentially entails computation of corresponding likelihoods for AR(1) models and fGns. Computation of likelihood functions for autoregressive processes is straightforward using standard time series techniques. Effective computation of the likelihood function for fGns can be achieved using the Durbin–Levinson algorithm for inverting the covariance matrix (McLeod et al. 2007).

In this paper the parameters of the two models are estimated by maximizing Eqs. (B1) and (B2) numerically.

## REFERENCES

- Aldrin, M., M. Holden, P. Guttorp, R. B. Skeie, G. Myhre, and T. K. Berntsen, 2012: Bayesian estimation of climate sensitivity based on a simple climate model fitted to observations of hemispheric temperatures and global ocean heat content. *Environmetrics*, **23**, 253–271, doi:10.1002/env.2140.
- Beran, J., 1994: *Statistics for Long-Memory Processes*. Chapman & Hall/CRC, 315 pp.
- Brohan, P., J. J. Kennedy, I. Harris, S. F. B. Tett, and P. D. Jones, 2006: Uncertainty estimates in regional and global observed temperature changes: A new data set from 1850. *J. Geophys. Res.*, **111**, D12106, doi:10.1029/2005JD006548.
- Crowley, T. J., 2000: Causes of climate change over the past 1000 years. *Science*, **289**, 270–277, doi:10.1126/science.289.5477.270.
- Embrechts, P., and M. Maejima, 2002: *Selfsimilar Processes*. Princeton University Press, 152 pp.
- Foster, G., and S. Rahmstorf, 2011: Global temperature evolution 1979–2010. *Environ. Res. Lett.*, **6**, 044022, doi:10.1088/1748-9326/6/4/044022.
- Geoffroy, O., D. Saint-Martin, D. J. L. Olivié, A. Voltaire, G. Bellon, and S. Tytéca, 2013: Transient climate response in a two-layer energy-balance model. Part I: Analytical solution and parameter calibration using CMIP5 AOGCM experiments. *J. Climate*, **26**, 1841–1857, doi:10.1175/JCLI-D-12-00195.1.
- Hansen, J., and Coauthors, 2005: Efficacy of climate forcings. *J. Geophys. Res.*, **110**, D18104, doi:10.1029/2005JD005776.
- , M. Sato, P. Kharecha, and K. von Schuckmann, 2011: Earth's energy imbalance and implications. *Atmos. Chem. Phys.*, **11**, 13 421–13 449, doi:10.5194/acp-11-13421-2011.
- Held, I. M., M. Winton, K. Takahashi, T. Delworth, F. Zeng, and G. K. Vallis, 2010: Probing the fast and slow components of global warming by returning abruptly to preindustrial forcing. *J. Climate*, **23**, 2418–2427, doi:10.1175/2009JCLI3466.1.
- Kantelhardt, J. W., E. Koscielny-Bunde, H. H. A. Rego, S. Havlin, and A. Bunde, 2001: Detecting long-range correlations with detrended fluctuation analysis. *Physica A*, **295**, 441–454, doi:10.1016/S0378-4371(01)00144-3.
- Lean, J. L., and D. H. Rind, 2009: How will Earth's surface temperature change in future decades? *Geophys. Res. Lett.*, **36**, L15708, doi:10.1029/2009GL038932.
- Lovejoy, S., 2013: What is climate? *Eos, Trans. Amer. Geophys. Union*, **94** (1), 1–2, doi:10.1002/2013EO010001.
- , and D. Schertzer, 2013: *The Weather and Climate: Emergent Laws and Multifractal Cascades*. Cambridge University Press, 489 pp.
- Mandelbrot, B., and J. W. van Ness, 1968: Fractional Brownian motions, fractional noises and applications. *SIAM Rev.*, **10**, 422–437, doi:10.1137/1010093.
- Mann, M. E., 2011: On long-range dependence in global temperature series. *Climatic Change*, **107**, 267–276, doi:10.1007/s10584-010-9998-z.
- McLeod, I. A., H. Yu, and Z. L. Krougly, 2007: Algorithms for linear time series analysis: With R package. *J. Stat. Software*, **23** (5), 1–26.
- Meehl, G. A., W. M. Washington, C. M. Amman, J. M. Arblaster, T. M. Wigley, and C. Tebaldi, 2004: Combinations of natural and anthropogenic forcings in twentieth-century climate. *J. Climate*, **17**, 3721–3727, doi:10.1175/1520-0442(2004)017<3721:CONAAF>2.0.CO;2.
- Moberg, A., D. M. Sonechkin, K. Holmgren, N. M. Datsenko, and W. Karlén, 2005: Highly variable Northern Hemisphere temperatures reconstructed from low- and high-resolution proxy data. *Nature*, **433**, 613–617, doi:10.1038/nature03265.

- Øksendal, B. K., 2003: *Stochastic Differential Equations: An Introduction with Applications*. Springer, 360 pp.
- Østvand, L., T. Nilsen, K. Rypdal, D. Divine, and M. Rypdal, 2014: Long-range memory in millennium-long ESM and AOGCM experiments. *Earth Syst. Dyn. Discuss.*, **5**, 363–401, doi:[10.5194/esdd-5-363-2014](https://doi.org/10.5194/esdd-5-363-2014).
- Otto, A., and Coauthors, 2013: Energy budget constraints on climate response. *Nature Geosci.*, **6**, 415–416, doi:[10.1038/ngeo1836](https://doi.org/10.1038/ngeo1836).
- Rybski, D., A. Bunde, S. Havlin, and H. von Storch, 2006: Long-term persistence in climate and the detection problem. *Geophys. Res. Lett.*, **33**, L06718, doi:[10.1029/2005GL025591](https://doi.org/10.1029/2005GL025591).
- Rypdal, K., 2012: Global temperature response to radiative forcing: Solar cycle versus volcanic eruptions. *J. Geophys. Res.*, **117**, D06115, doi:[10.1029/2011JD017283](https://doi.org/10.1029/2011JD017283).
- , L. Østvand, and M. Rypdal, 2013: Long-range memory in Earth's surface temperature on time scales from months to centuries. *J. Geophys. Res.*, **118**, 7046–7062, doi:[10.1002/jgrd.50399](https://doi.org/10.1002/jgrd.50399).
- Schurer, A. P., S. F. B. Tett, and G. C. Hegerl, 2014: Small influence of solar variability on climate over the past millennium. *Nat. Geosci.*, **7**, 104–108, doi:[10.1038/ngeo2040](https://doi.org/10.1038/ngeo2040).
- Solomon, S., D. Qin, M. Manning, Z. Chen, M. Marquis, K. Averyt, M. Tignor, and H. L. Miller Jr., Eds., 2007: *Climate Change 2007: The Physical Science Basis*. Cambridge University Press, 996 pp.
- Stocker, T. F., and Coauthors, Eds., 2013: *Climate Change 2013: The Physical Science Basis*. Cambridge University Press, 1535 pp.